doi:10.1006/jmbi.2001.5321 available online at http://www.idealibrary.com on IDEAL® *J. Mol. Biol.* (2002) **315**, 1219–1229

JMB

Solution Structure of the Eukaryotic Pore-forming Cytolysin Equinatoxin II: Implications for Pore Formation

Mark G. Hinds[1], Wei Zhang[2], Gregor Anderluh[3], Poul Erik Hansen[2] and Raymond S. Norton[1]*

[1]*Biomolecular Research Institute, 343 Royal Parade Parkville 3052, Australia*

[2]*Institute of Life Sciences and Chemistry, Roskilde University Denmark*

[3]*Biotechnical Faculty Department of Biology University of Ljubljana 1000 Ljubljana, Slovenia*

**Corresponding author*

Sea anemones produce a family of 18-20 kDa proteins, the actinoporins, that lyse cells by forming pores in cell membranes. Sphingomyelin plays an important role in their lytic activity, with membranes lacking this lipid being largely refractory to these toxins. The structure of the actinoporin equinatoxin II in aqueous solution, determined from NMR data, consists of two short helices packed against opposite faces of a β-sandwich structure formed by two five-stranded β-sheets. The protein core has extensive hydrophobic interfaces formed by residues projecting from the internal faces of the two β-sheets. ^{15}N relaxation data show uniform backbone dynamics, implying that equinatoxin II in solution is relatively rigid, except at the N terminus; its inferred rotational correlation time is consistent with values for monomeric proteins of similar mass. Backbone amide exchange rate data also support the view of a stable structure, even though equinatoxin II lacks disulfide bonds. As monitored by NMR, it unfolds at around 70 °C at pH 5.5. At 25 °C the structure is stable over the pH range 2.5-7.3 but below pH 2.5 it undergoes a slow transition to an incompletely unfolded structure resembling a molten globule. Equinatoxin II has two significant patches of positive electrostatic potential formed by surface-exposed Lys and Arg residues, which may assist its interaction with charged regions of the lipid head groups. Tyr and Trp residues on the surface may also contribute by interacting with the carbonyl groups of the acyl chains of target membranes. Data from mutational studies and truncated analogues identify two regions of the protein involved in membrane interactions, the N-terminal helix and the Trp-rich region. Once the protein is anchored, the N-terminal helix may penetrate the membrane, with up to four helices lining the pore, although other mechanisms of pore formation cannot be ruled out.

Keywords: cytolysin; sea anemone; toxin; β-sheet; pore formation

Introduction

Sea anemones produce a family of toxins, the actinoporins, that function by forming pores in cell membranes.[1–3] These highly basic proteins, with molecular masses in the range 18-20 kDa, display permeabilising activity in model lipid and cell membranes that is markedly enhanced by the presence of sphingomyelin. In contrast to bacterial pore-forming toxins such as staphylococcal α-toxin and the leukocidin family,[4] aerolysin and related toxins from *Aeromonas*,[5] colicins[6] and cholesterol-dependent cytolysins,[7] there is little detailed information on the mechanism of action of these toxins. Actinoporins differ from these toxins in several respects: they are more potent, the pore they form does not have a stable structure and has not yet been visualized directly, and they are of smaller

Present addresses: M. G. Hinds and R. S. Norton, The Walter and Eliza Hall Institute of Medical Research, P. O. Royal Melbourne, Parkville, VIC 3050, Australia.

Abbreviations used: EqTII, equinatoxin II; ANS, 2-anilinonaphthalene-6-sulfonic acid; CD, circular dichroism; IR, infrared; NOE, nuclear Overhauser effect; RMS, root mean square; FTIR, Fourier transform infrared; NOESY, NOE spectroscopy.

E-mail address of the corresponding author: rnorton@wehi.edu.au

0022-2836/02/051219–11 $35.00/0

size and extremely stable towards proteolytic degradation. Indeed, the potency and properties of these cytolysins have prompted their evaluation as the toxic component of chimeric proteins targeted at tumour cells[8,9] and human parasites.[10] The nature of their interaction with lipids in bilayer membranes and the specific role of sphingomyelin in pore formation are not understood at the molecular level.

In common with many pore-forming toxins, the actinoporins are highly water-soluble, stable proteins, and yet their only known activity is the formation of oligomeric pores in membranes. Early estimates that three to four monomers were required to form a functional pore[11,12] have been supported by more recent data.[13–15] Moreover, tetramers of the actinoporin sticholysin II have been observed in solution[16] and when crystallized on lipid monolayers.[17] The resulting pores have a radius of about 1 nm[13,15,"18] and are permeable to small molecules and solutes, with the resulting osmotic imbalance promoting cell lysis.

Sphingomyelin plays an important role in the lytic activity of the actinoporins. Bernheimer and colleagues showed that the haemolytic activity of a cytolysin from *Stoichactis* (now *Stichodactyla*) *helianthus* was inhibited by pre-incubation with sphingomyelin and that treatment of erythrocyte membranes with sphingomyelinase rendered them resistant to lysis by this toxin.[19,20] Furthermore, a toxin-ferritin conjugate was observed by electron microscopy to bind to liposomes containing sphingomyelin but not to those containing only phosphatidylcholine.[20] More recent studies with sticholysins I[14] and II[15] on model membranes have confirmed that sphingomyelin enhances lytic activity and also suggested that cholesterol may have a minor role.[15] A detailed study of the interaction of equinatoxin II (EqTII) with model membranes[21] showed that the toxin could bind to large unilamellar vesicles containing phosphatidylcholine but the association was reversible and did not involve major conformational changes. The presence of sphingomyelin enabled irreversible insertion and pore formation, which were associated with major conformational changes. Some EqTII-induced leakage was observed from large unilamellar vesicles containing only phosphatidylcholine and cholesterol, again suggesting a contribution of this lipid to actinoporin cytolytic activity, albeit a much less significant one than that of sphingomyelin. Fluorescence studies of EqTII binding to lipid vesicles showed that association was markedly enhanced by the presence of sphingomyelin.[22]

Equinatoxin II, the subject of this paper, is a 179-residue, 19.8-kDa cytolysin isolated from the Mediterranean anemone *Actinia equina* L.[23] It is essentially identical with tenebrosin-C, a cytolysin isolated from the Australian red waratah anemone *Actinia tenebrosa*,[24] and the first of this class of toxins to be sequenced in full;[25] tenebrosin-C has a variant S177T and EqTII a variant P81D.[26] EqTII and tenebrosin-C show a high degree of sequence similarity (>60 %) to cytolysins of *Stichodactyla helianthus, Heteractis magnifica* and other sea anemones.[1,2,27–29] The structure was predicted to be predominantly β-sheet but with helices at the N and C termini.[25] This mix of β-sheet and helical structures has been confirmed by various spectroscopic analyses, including CD[26,30,31] and IR.[21,32]

There is evidence of a slight conformational change upon binding to the membrane in EqTII and related actinoporins. CD and FTIR studies both detected small increases in β-sheet and α-helical content at the expense of random structure in the presence of unilamellar vesicles.[18,31,33] Somewhat surprisingly, recent IR studies[21] found a decrease in α-helical content and a significant increase in β-sheet in large unilamellar vesicles consisting of 1:1 phosphatidylcholine and sphingomyelin. Using Cys-scanning mutagenesis, Anderluh *et al*.[34] concluded that at least two regions of EqTII became embedded in lipid membranes, the N-terminal region (residues 13-20) and the Trp-rich region (residues 105-120). The partition of the Trp-rich region was supported by a recent study using single Trp mutants.[32]

Our goal is to determine a high-resolution structure for EqTII both in solution and in a membrane environment. We also wish to elucidate the structural basis for its interaction with sphingomyelin, which appears to be a necessary constituent of membranes susceptible to lysis by EqTII, and to understand how it oligomerises to form pores. Here we describe its structure and dynamics in aqueous solution, and the effects of pH and temperature. The structure provides the basis for interpretation of a large body of physicochemical data in the literature, as well as a starting point for experiments designed to probe its interaction with lipid membranes.

Results

Structure determination

Essentially complete, sequence-specific, backbone and side-chain assignments for the ^{1}H, ^{13}C and ^{15}N resonances of double-labelled EqTII have been described.[35] Analytical ultracentrifugation showed that EqTII was monomeric at pH 5.1 and 7.4 and ca 0.05 mM protein in 50 mM acetate and phosphate buffers, respectively, each containing 50 mM NaCl (calculated masses 19,400 and 19,990, respectively, assuming a partial specific volume of 0.73×10^{-3} m^3 kg^{-1} and solvent density of 1×10^3 kg m^{-3}; theoretical mass 19,819). As the linewidths and relaxation data (see below) were also consistent with a monomer, NMR restraints were interpreted on this basis.

The final structure set was calculated with CNS[36] after final NMR constraints were derived iteratively using DYANA.[37] The final family of 20 structures was selected after energy minimisation in a box of water using the OPLSX non-bonded

parameters of Linge & Nilges.[38] Parameters characterising the final 20 structures and structural statistics are summarised in Table 1, and a superposition of the final 20 structures is shown in Figure 1. Residues 8-12, 14-25, 29, 31-40, 42-45, 48-53, 56, 60, 65, 67-74, 86-95, 98-107, 113-121,128-132, 141-142, 146, 150-154, 159-162, 164-165 and 169-177, were well defined according to their backbone angular order parameters ($S(\phi)$ and $S(\psi) \geqslant 0.9$), and the structures shown in Figure 1 were superimposed over the backbone atoms N, C^{α} and C of residues from the β-sandwich. PROCHECK[39] analysis of the NMR ensemble indicates that 83% of the ordered residues lie in the most favourable regions of the Ramachandran plot while for all residues 72% lie in these regions. The data in Table 1 show that the ensemble of NMR structures is energetically reasonable and has acceptable covalent geometry.

The less well-defined regions of the structure, residues 1-6, 79-82, 110-111 and 134-138, are thus mainly because of incomplete resonance assignments. At the N terminus the incomplete assignments reflect a lack of NOEs for residues 1-6, which in turn probably arises because this region is flexible and extends away from the rest of the molecule. A dearth of NOE restraints for Glu134 and Glu135, particularly the latter, accounts for the poorer definition around residues 134-138, but the relaxation data presented below indicate that this segment is no more flexible that the rest of the protein. Missing assignments for Asp78 and Asp109 affect the regions 79-82 and 110-111, respectively. Other than the N terminus, only residues 79-82 appear to owe their poorer definition to greater flexibility, as described below.

Description of structure

As illustrated in Figure 2, the structure consists of two short helices packed against opposite faces of a β-sandwich type structure formed by two five-stranded β-sheets. The core of the protein has extensive hydrophobic interfaces formed by residues projecting from the internal faces of the two β-sheets. The N-terminal helix (α1, residues 15-26) packs against a β-sheet formed by strands β1 (32-40), β3 (69-75), β8 (150-154), β9 (158-165) and β10 (170-177). Strand β1 lies between β3 and β10 and is antiparallel to β3 but parallel to β10, while β8, β9 and β10 are antiparallel. The second short α-helix, α2 (129-134), lies between strands β6 and β7 and is approximately normal to the antiparallel β-sheet formed by strands β2 (46-53), β4 (86-94), β5 (98-106), β6 (115-124) and β7 (143-145). The hydrophobic surface of helix α1 and Leu14 make contact with the non-polar face of the β-sheet. Leu19 and Leu23 in helix α1 are almost entirely buried and make contact with residues on strands β1, β3 and β10 while Val22 makes contacts with Ala34 and Asn74 on β1 and β3, respectively. Likewise, helix α2 is anchored to the sheet by interactions involving Asp129 and two tyrosine residues, Tyr51 and

Table 1. Summary of restraints and structural statistics for the 20 lowest energy structures of EqTII in aqueous solution at pH 3.9 and 30 °C following minimization in water[38] using CNS[36]

Experimental constraints		
Total		3161
Sequential ($\|i-j\|=1$)		634
Short range ($1<\|i-j\|<5$)		972
Long range ($\|i-j\| \geqslant 5$)		1346
Hydrogen bonds		42
Dihedral angles (120φ, 47ψ)		167
Rmsd from experimental distance restraints (Å)	0.0223 ± 0.0015	
Rmsd from experimental dihedral restraints (deg.)	0.404 ± 0.057	
Rmsd from idealized covalent geometry		
Bonds (Å)	0.00424 ± 0.00018	
Angles (deg.)	0.579 ± 0.020	
Impropers (deg.)	0.455 ± 0.023	
Measures of structural quality		
E_{LJ} (kcal mol^{-1})	-799 ± 39	
Procheck % residues in region of Ramachandran plot (ordered residues $S(\phi)$ and $S(\psi) \geqslant 0.9$)		
Most favourable		71.7 (82.8)
Additionally allowed		22.3 (15.7)
Generously allowed		3.7 (1.3)
Disallowed		2.4 (0.3)
Angular order: residues with $S(\phi) \geqslant 0.9$		129
With $S(\psi) \geqslant 0.9$		119
Bad contacts per 100 residues	0.6 ± 0.8	
Coordinate precision		
Mean pairwise RMSD (Å)	C^{α}, C, N	All heavy atoms
Residues		
Residues 6-179	1.59 ± 0.25	2.75 ± 0.31
All secondary structure	1.40 ± 0.24	2.30 ± 0.22
β1-β10	0.71 ± 0.14	1.66 ± 0.15

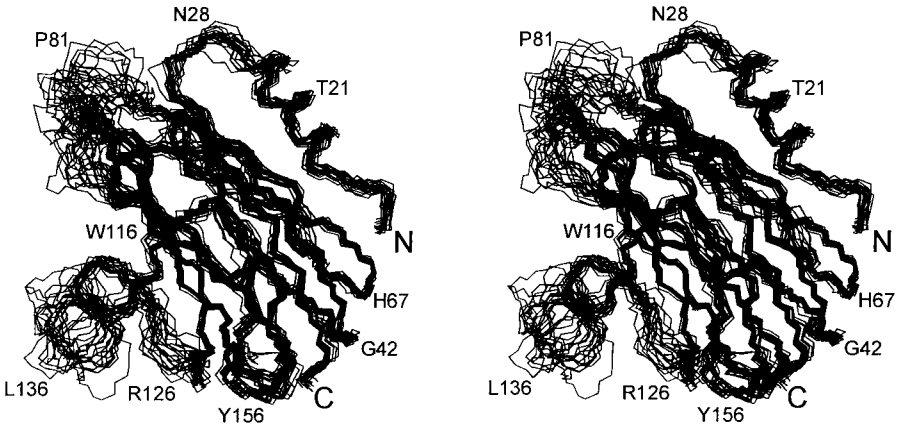

Figure 1. Stereo view of family of 20 structures of EqTII superimposed over the backbone heavy atoms (N, C^{α}, C) of the β-strands (β1 residues 32-40, β2 46-53, β3 69-75, β4 86-94, β5 98-106, β6 115-124, β7 143-145, β8 150-154, β9 158-165 and β10 170-177).

Tyr122, projecting from strands β2 and β6, respectively.

The locations of the five Trp and 11 Tyr residues are also shown in Figure 2(a). The indole rings of Trp112, 116 and 149 are exposed to solvent whereas those of Trp45 and 117 are buried. A remarkable feature of the surface of EqTII is the presence of several clusters of aromatic side-chains, as illustrated in Figure 2(a). In the eight-residue loop connecting strands β5 and β6 there are four highly solvent-accessible aromatic residues, Tyr108, Tyr110, Trp112 and Tyr113, while projecting from α2 are Tyr137 and Tyr138.

EqTII is a highly basic molecule, with 11 Lys and ten Arg balanced by ten Asp and five Glu. Two views of a GRASP representation of the molecular surface (Figure 2(b)) reflect this, with a predominance of positive potential evident. In particular, there is one major cluster of positively charged side-chains centred on Arg53, 120, 152 and Lys123, 159, 178, and a smaller one nearby involving the tripeptide sequence Lys125-Arg126-Arg127. As discussed below, both the aromatic and positively charged regions of the surface may play a role in membrane interactions of EqTII.

While this manuscript was in preparation, the crystal structure of EqTII at 1.9 Å resolution was published.[40] The two structures are in close agreement, with an RMSD of 2.68 Å over the backbone heavy atoms of residues 5-179 and 1.57 Å over the 145 residues judged to be structurally closest by the structure comparison program TOP[41] (residues 8-57, 62-79, 83-95, 97-111, 113-123, 129-131, 141-153, 156-162, 164-166, 168-179). The first four residues were not defined in the crystal structure, in agreement with our observation that the N terminus is disordered in solution. The most significant difference between the NMR and X-ray-derived structures lies between residues 134-138 located in the loop connecting strands β6 and β7 and containing helix α2. Two residues in this region, Glu134 and Glu135, have few long-range restraints and consequently are poorly ordered in solution. In the crystal structure[40] α2 residues pack against the corresponding region in a crystallographic symmetry-related molecule, and this may have some effect on the structural order in this region of the crystal structure. Generally, however, the secondary structures agree well, having the lowest RMSD.

Dynamics

As shown in Figure 3, ^{15}N relaxation rates and ^{15}N NOEs show uniform backbone dynamics, implying that EqTII in solution behaves as a relatively rigid molecule, except at the N terminus and around Gly80. The average ^{15}N T_1 and T_2 values of 762 ms and 77 ms, respectively, correspond to an effective correlation time of 9.6 ns on the assumption of isotropic overall reorientation, consistent with values for proteins of similar size that are also monomeric.[42] As the goal of these measurements was simply to identify flexible regions of the structure, a more detailed analysis of these relaxation data was not undertaken.

A total of 71 backbone amide protons was identified in a 2D HSQC spectrum recorded two days after dissolution in $^{2}H_2O$ at 20 °C. Of these, 24 gave weak peaks and are classified as having intermediate exchange rates and the remaining 47 gave strong peaks consistent with slow exchange, as shown in Figure 3; for the purpose of discussion these 71 amides are considered as a single group. Many of these 71 amides are from regions with ordered secondary structure, but a significant number are from loop regions. Several continuous sequences of slowly exchanging amide protons are observed, including residues 32-41, 88-94, 97-106 and 139-145 (allowing for the presence of Pro142), which correspond to β-sheet strands 1, 4 and 5, as well as β-strand 7 and the region immediately pre-

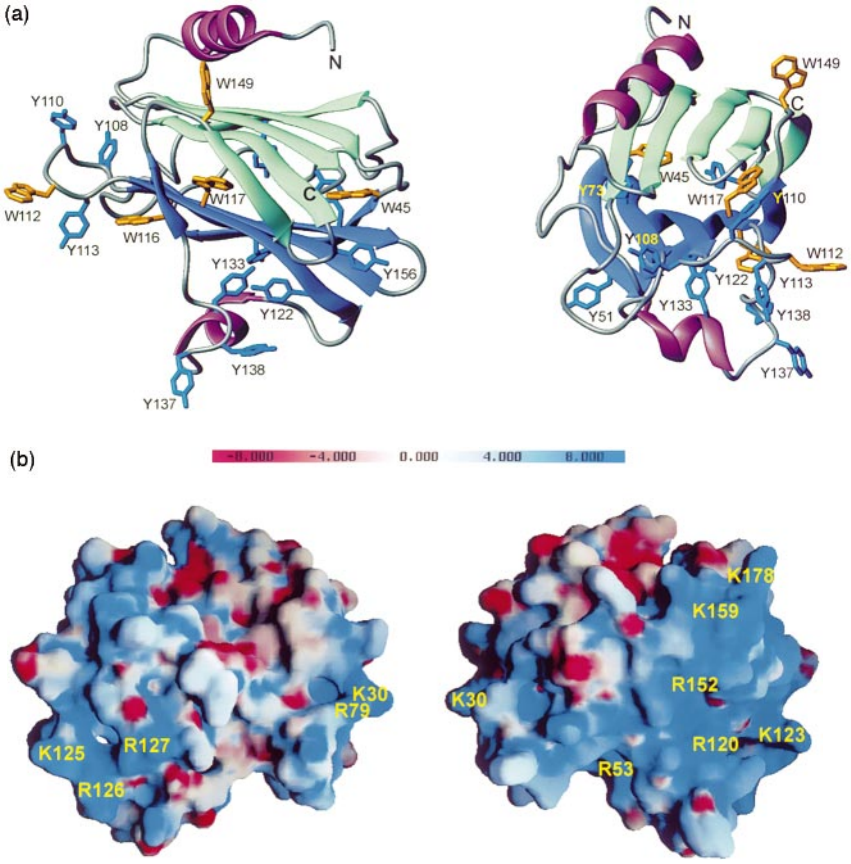

Figure 2. (a) Ribbon diagram generated using MOLMOL[62] of structure closest to the mean showing elements of secondary structure with the Trp residues depicted in orange and the Tyr residues in blue. The right-hand view is related to the left by a 90° rotation about the vertical axis and a slight tilt towards the viewer. (b) Surface charge potential distribution on EqTII showing two views related by a 180° rotation about the vertical axis. The right-hand image depicts a similar view to the left-hand image of (a). Areas of negative potential are coloured red and positive potential blue. This Figure was created using the program GRASP.[63] The potential is displayed over the range $<-8k_bT$ and $>+8k_bT$, where k_b is the Boltzmann constant and T the temperature.

ceding it. These four regions are also characterised by their high hydrophobicity, with sequences of non-polar residues spanning positions 33-37, 86-94 and 100-104 and 136-140.

Six of the C-terminal ten residues are also slowly exchanging, indicating that the C-terminal β-strand (β10) is tightly associated with the bulk of the structure. By contrast, of the first 30 residues, only 13, 18 and 24 are slowly exchanging, confirming that this region of the protein, which includes the α1 helix, is less tightly associated with the rest of the structure.

The longest internal loop in the structure spans residues 124-146 and encompasses the α2 helix and the short β7 strand. The relaxation data indicate that it is not undergoing fast internal motions (on the picosecond to nanosecond time scale) relative to the rest of the protein. The observation that nearly half of the backbone amides from this region are in slow exchange with solvent indicates that it is also rigid on the millisecond to second time scale. Amide protons with slow or very slow exchange rates are also found in other regions lacking ordered secondary structure, for example residues 13, 61 and 65.

Effects of temperature and pH

One-dimensional ^{1}H NMR spectra of 0.1 mM EqTII at pH 5.5 showed that the structure was unchanged up to 65 °C but unfolded between 65 and 75 °C to give a spectrum with no fine structure or shifted resonances. After cooling to 25 °C the spectrum was consistent with a mixture of native and denatured protein, indicating that thermal denaturation is only partially reversible. 1D spectra of a 0.2 mM solution showed no evidence of conformational changes over the pH 2.5-7.3 at 25 °C. At higher pH values the protein began to aggregate. 2D NOESY spectra of a 1 mM solution showed that the native structure was retained down to pH 2.5. At pH 1.8 initial 1D spectra were consistent with a mixture of native structure and a partially denatured state. Over a period of two days 1D spectra showed a steady decrease in the content of native structure (to less than a third of its initial level). The two conformations of the protein at this pH were in slow exchange on the NMR time scale, with clearly distinct sets of resonances being observed. The possibility that the initial spectrum at pH 1.8 represents a single state of the protein containing some elements of native structure cannot be ruled out entirely, but seems less likely given that the location and number of the dispersed resonances were similar to that seen at higher pH values. A mixture of native and non-native conformations of the protein, with a slow transition from the former to the latter is the more likely scenario. The non-native state exhibited limited spectral dispersion but not the sharp reson-

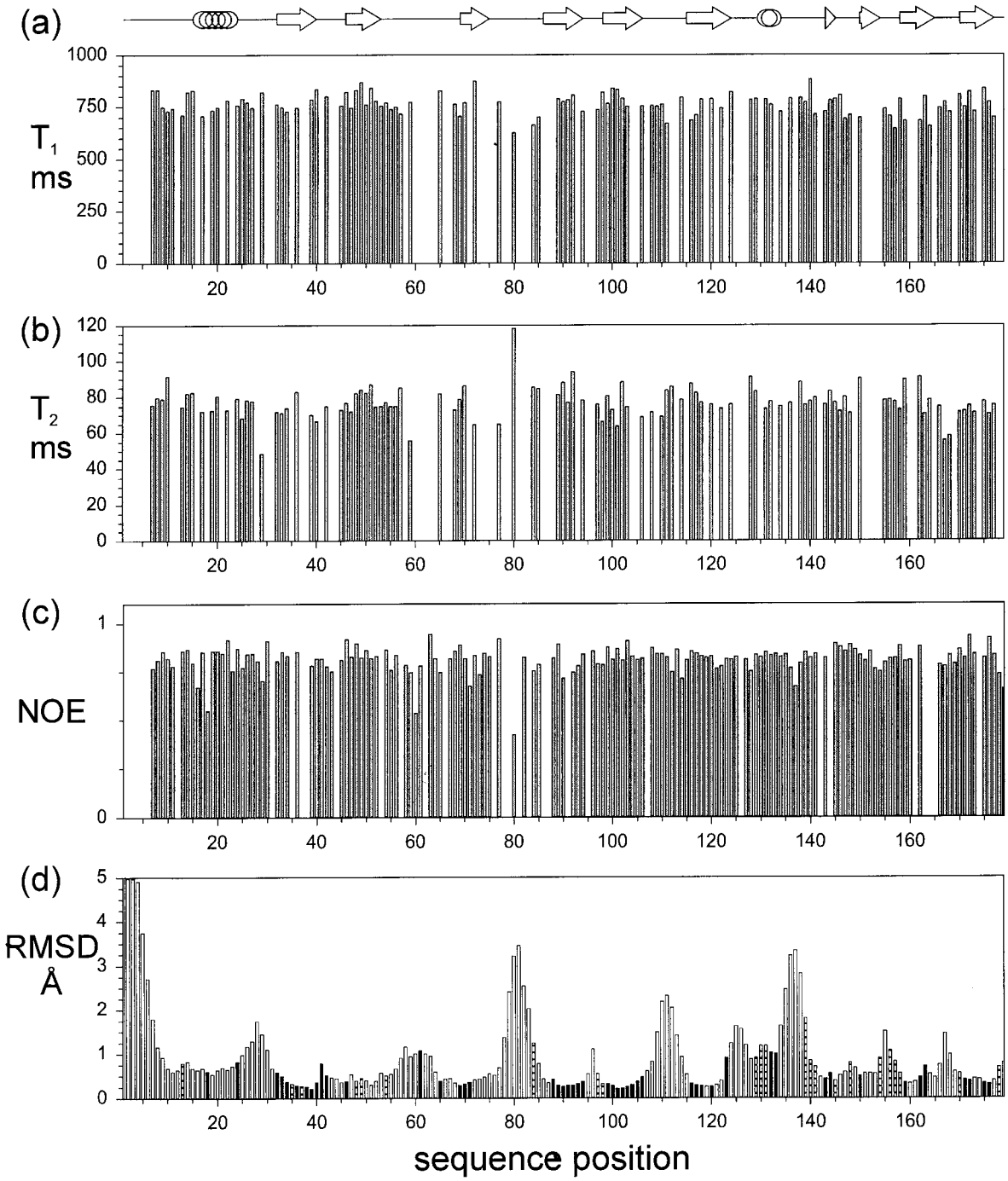

Figure 3. Summary of backbone ^{15}N relaxation parameters T_1 (a), T_2 (b) and steady-state $\{^1H\}$-^{15}N NOE (c) for EqTII recorded at 30 °C and ^{15}N frequency −60.81 MHz. Gaps in the data arise mainly from peak overlap in the 2D spectra. This is the case for residues 78 and 79, which precede the apparently flexible Gly80; residue 81 is a proline. The data shown are from a single set of measurements in each case, with an estimated accuracy of better than 10%. (d) RMS deviations from the mean structure for the backbone heavy atoms (N, C^α, C) following superposition over residues from the β-sandwich. The locations of the 47 slowly exchanging backbone amide protons are shown in (d) as filled bars and the 24 with intermediate exchange rates as striped bars.

ances normally associated with a random coil; moreover, it gave strong NOESY cross-peaks. These properties are consistent with a molten globule structure for the acid-denatured state, although they could also be accounted for by an unfolded and aggregated form of the protein. When the pH was raised to 2.0 the initial 1D spectrum was similar to the final spectrum at pH 1.8 and there was only slight recovery of the native spectrum over a further two days. At pH 2.3 recovery was still incomplete.

Discussion

The structure of EqTII in aqueous solution is well-defined except for a few residues at the N terminus, and, according to both backbone ^{15}N relaxation data and backbone amide exchange measurements, relatively rigid. In this section we compare the EqTII structure with related structures and consider how the structure might change as it makes the transition from a water-soluble, monomeric protein to an oligomeric, membrane-bound pore.

Related structures

Database searches using Dali[43] and VAST[44] show that the most similar structure to EqTII is thaumatin (Dali *Z* score 3.2, PDB code 1thv). Thaumatin is a sweet-tasting protein that is not known to form pores, but it shows sequence similarity to plant ''pathogenesis-related'' proteins (PR-5 group) which do.[45] One interesting but distantly related protein (*Z* score 2.4, PDB code 1svb) is domain I of the envelope glycoprotein from tick-borne encephalitus virus.[46] The envelope glycoprotein lies parallel to the viral surface and domain I, a nine-stranded β-barrel, lies on the exposed viral membrane face. Helix α1 of EqTII lies on the structurally equivalent β-sheet, so a mechanism of pore formation in which this helix penetrated the membrane and the β-sandwich lay on the membrane surface anchored by aromatic residues, as discussed below, would strengthen this similarity. There is some overall structural similarity between thaumatin and the envelope glycoprotein but the positions of solvent-exposed aromatic residues are not maintained across the three structures.

Another membrane-active protein, perfringolysin O, also shows weak structural similarity to EqTII (*Z* score 2.3, PDB code 1pfo). As noted by Athanasiadis *et al.*[40], domain IV of perfringolysin O is similar to EqTII and essential for membrane interactions. Other proteins not known to be membrane-active, such as a papain complex (*Z* score 2.8, PDB code 1stf-I) and major sperm protein msp (*Z* score 2.5, PDB code 1msp-A), also have weak similarity to EqTII.

Interaction with membranes

In the transition from monomeric, water-soluble EqT II to a functional pore at least two steps must occur: binding of the protein to the surface of the membrane and subsequent oligomerisation to form a channel. Changes in the structure of the toxin could occur upon initial association with the membrane and then again as the membrane-bound monomer associates to form the pore. CD and FTIR studies detected small increases in β-sheet and α-helical content at the expense of random structure in the presence of unilamellar vesicles.[18,31,33] Using Cys-scanning mutagenesis, Anderluh *et al.*[34] concluded that at least two regions of EqTII became embedded in lipid membranes, the N-terminal region (residues 13-20) and the Trp-rich region (residues 105-120). The importance of the N-terminal helix to pore formation is emphasized by truncation studies,[47] with truncated analogues lacking five or ten N-terminal residues having 89 and 31 % of native haemolytic activity, respectively, and an analogue lacking 33 N-terminal residues having none.

A large patch of positive electrostatic potential formed by the surface-exposed residues Arg120, Lys123, Arg152, Lys159 and Lys178, together with the contiguous sequence Lys125-Arg126-Arg127, (Figure 2(b)) may assist the interaction of EqTII with charged regions of the lipid head groups. A separate and smaller patch of positive electrostatic potential is centred on Lys30 and Arg79 (Figure 2(b)). Of even greater interest is the abundance of Tyr and Trp residues on the surface of EqTII, as these residues are well known to play a role in anchoring proteins in the hydrocarbon-water interface region of the membrane,[48] possibly *via* interaction with the carbonyl groups of the acyl chains. As shown in Figure 2(b), Tyr110, Trp112, Trp113 and Trp116 form one cluster on the surface, and Tyr137 and Tyr138, possibly with a contribution from Tyr133, another. One or both of these aromatic clusters may anchor EqTII in the membrane, assisted by interactions of the positively charged side-chains referred to above with the charged region of the lipid head groups at the surface of the membrane. Associated with this interaction, the N-terminal helix could then penetrate the membrane, with three, or more likely four, helices lining the pore. With only 12 residues, the N-terminal helix is shorter than the 25 or so required to span a membrane in a helical conformation, but the first strand of sheet does not commence until Lys32, so there is ample scope for formation of additional helix in the N terminus without disrupting the sheet, and small increases in helical content are observed upon membrane binding.[18,31,33] Indeed, EqTII may form a toroidal pore of the type proposed recently for magainin and melittin[49] and suggested for sticholysins I and II.[50]

An alternative mechanism of pore formation derives from the structure of α-haemolysin,[51] a heptameric protein that forms trans-membrane pores consisting of a 14-stranded antiparallel β-barrel with two strands contributed by each monomer. In the case of EqTII, such a trans-membrane pore could consist of four β-hairpins, one from each monomer, encompassing residues 118-142, with a turn around residue 130 and flanked by sequences 107-118 and 142-148. The hairpin would include β-strands 6 and 7 and helix α2, and would require a more significant conformational rearrangement upon membrane binding than the model described above, with the β-strand 6 having to unzip from the β-sheet to form the hairpin. The putative β-hairpin does, however, incorporate the Tyr/Trp-rich region.

Conformational stability

Following the reasoning that conformational changes seen upon association with lipid membranes may resemble to some degree those in the aqueous state of EqTII under mild denaturing conditions, several studies have been carried out. Poklar *et al.*[30] found that EqTII maintains its native conformation at pH 5.5-6.0 and <60 °C, but at higher temperatures undergoes a collapse of tertiary structure and an incomplete denaturation of secondary structure. At pH 2.0 the low-temperature initial state is already partially denatured, while at pH 1.1 and <60 °C, EqTII exists in a stable acid-denatured compact state with the characteristics of a molten globule (absence of defined tertiary structure, increase in α-rich secondary structure, high affinity for ANS). More recently, the structure was found to be stable between pH 7 and 2, but below pH 2 a native-to-partially unfolded transition occurs.[52] Above 50 °C, the acid-induced denatured state of EqTII reversibly denatures to a more unfolded state.

Is it possible that partially folded states of EqTII contribute to its pore-forming ability? Our NMR studies confirm that the molecule undergoes a conformational transition at low pH to a state with properties consistent with those of a molten globule; around pH 2 this transition occurs over a period of days. The molten globule is attractive as a potential intermediate in membrane binding as it retains secondary structure but has a loosened overall structure. An interesting comparison may be drawn with the pore-forming domain of colicin A, a water-soluble bacterial toxin. The apparent p*K* for its insertion into membranes is around 4.8 but in solution it forms a molten globule with a p*K* around 2.7.[53] It eventuates that the pH at the surface of negatively charged vesicles differs by up to 1.6 units from that of the bulk solution because of the electric surface potential,[53] and this is sufficient to implicate the molten globule state of colicin A in membrane binding. EqTII shows maximum lytic activity around pH 8-9, although an increased membrane interaction around pH 4 was noted.[13] The population of the acidic molten globule state at pH 8-9 would be small but it would be interesting to assess the activity of EqTII mutants in which formation of the molten globule was favoured.

The role of sphingomyelin in pore formation remains to be elucidated. It seems clear that the presence of sphingomyelin is not an absolute requirement for lytic activity of the actinoporins, but it significantly enhances this activity. Whether this is the result of a direct interaction between EqTII and sphingomyelin, favouring the membrane-bound and/or oligomeric forms of the protein, remains to be established, but NMR studies of the interaction between EqTII and water-soluble analogues of sphingomyelin should define the nature of this association. An alternative explanation is that EqTII may prefer to bind to lipid rafts in biological membranes, which are known to contain sphingolipids and cholesterol.[54] Thus, the physical environment within these lipid rafts may be conducive to EqTII binding and oligomerisation without the need for any specific interaction between EqTII and sphingomyelin.

† (http://www.bmrb.wisc.edu)

Materials and Methods

NMR spectroscopy

EqTII was prepared in an *Escherichia coli* expression system[55] and uniformly labelled with ^{15}N or ^{13}C and ^{15}N as described.[35] Spectra were recorded on VARIAN Unity *Inova* 600 and 800 spectrometers and a Bruker DRX-600, all equipped with triple-resonance gradient probes. Protein concentration was ~1 mM, the pH 3.9, and the probe temperature 30 °C. DQF-COSY, TOCSY and NOESY spectra were acquired on an unlabelled protein sample, both in H_2O and ^2H_2O. ^{15}N HSQC, HNHA and ^{15}N-edited NOESY and TOCSY spectra were recorded on ^{15}N-labelled protein. HNCA, HN(CO)CA, HNCACB, HN(CO)CACB, HNCO, H(CC)-TOCSY-(CO)NH, CC-TOCSY-(CO)NH, HCCH-TOCSY experiments were recorded with ^{13}C,^{15}N-labelled protein.[56] NMR data were processed with the VNMR software and analysed using XEASY.[57] ^1H, ^{15}N and ^{13}C assignments have been deposited in the BioMagResBank database† with accession number 4797. ^{15}N {^1H} Heteronuclear NOE, T_1 and T_2 spectra[58] were recorded at 600 MHz.

Distance and angle restraints

Approximate inter-proton distances were derived from 2D-NOESY and 3D ^{13}C- and ^{15}N-edited NOESY spectra with mixing times of 120 ms. Backbone φ constraints were determined from $^3J_{HNHA}$ coupling constants determined from a HNHA spectrum[59] and ψ angles were restricted according to the value of the chemical shift of their C^α resonance.[60] Residues that were not restricted according to their $^3J_{HNHA}$ coupling constant were restricted in their φ angle as described by Luginbühl *et al.*[60] or to negative φ angles where the condition for a positive φ angle was not met.[61] Hydrogen bond constraints were applied at a late stage of the structure calculation where there existed the characteristic NOE patterns observed for α-helices or β-strands. For each hydrogen bond constraint, upper limits of 2.3 and 3.3 Å were used for the distances from proton to acceptor and donor nitrogen atom to acceptor, respectively.

Structure calculations and analysis

Initial structure calculations and optimisation of experimental distance and angle constraints were performed using DYANA v1.5.[37] Interproton distances were derived from NOE peak volumes with the CALIBA module within DYANA. Once the final set of experimental restraints had been obtained a new family of structures was generated using CNS v1.0[36] and refined using dynamic simulated annealing. The lowest 50 penalty function structures were selected from a calculation of 250 and minimised in a box of water using the OPLSX parameterisation.[38] Structural analysis was performed on the 20 structures with the lowest stereochemical energies,

and PROCHECK_NMR[39] was used for assessment of their stereochemical quality. The structures had no experimental distance violations greater than 0.3 Å or dihedral angle violations greater than 5°. Structural Figures were created using MOLMOL.[62]

Atomic coordinates

Coordinates for the final set of 20 structures have been deposited in the Protein Data Bank under accession number 1KD6.

Acknowledgements

We thank the Carlsberg Foundation for travel support for M.G.H., Geoff Howlett for analytical ultracentrifugation measurements and Frances Separovic for helpful discussions. Use of the facilities of the Danish Instrument Centre for NMR of Biological Macromolecules is acknowledged.

References

1. Turk, T. (1991). Cytolytic toxins from sea anemones. *J. Toxicol. - Toxin Rev.* **10**, 223-262.
2. Maček, P. (1992). Polypeptide cytolytic toxins from sea anemones (*Actinaria*). *FEMS Microbiol. Immunol.* **105**, 121-130.
3. Anderluh, G. & Maček, P. (2002). Cytolytic peptide and protein toxins from sea anemones (Anthozoa: Actiniaria). *Toxicon,* **40**, 111-124.
4. Prevost, G., Mourey, L., Colin, D. A. & Menestrina, G. (2001). Staphylococcal pore-forming toxins. *Curr. Top. Microbiol. Immunol.* **257**, 53-83.
5. Fivaz, M., Abrami, L., Tsitrin, Y. & van der Goot, F. G. (2001). Aerolysin from *Aeromonas hydrophila* and related toxins. *Curr. Top. Microbiol. Immunol.* **257**, 35-52.
6. Lakey, J. H. & Slatin, S. L. (2001). Pore-forming colicins and their relatives. *Curr. Top. Microbiol. Immunol.* **257**, 131-161.
7. Billington, S. J., Jost, B. H. & Songer, J. G. (2000). Thiol-activated cytolysins: structure, function and role in pathogenesis. *FEMS Microbiol. Letters,* **182**, 197-205.
8. Avila, A. D., Mateo de Acosta, C. & Lage, A. (1989). A carcinoembryonic antigen-directed immunotoxin built by linking a monoclonal antibody to a hemolytic toxin. *Int. J. Cancer,* **43**, 926-929.
9. Pederzolli, C., Belmonte, G., Dalla, Serra M., Maček, P. & Menestrina, G. (1995). Biochemical and cytotoxic properties of conjugates of transferrin with equinatoxin II, a cytolysin from a sea anemone. *Bioconjug. Chem.* **6**, 166-173.
10. Tejuca, M., Anderluh, G., Maček, P., Marcet, R., Torres, D., Sarracent, J. *et al.* (1999). Antiparasite activity of sea-anemone cytolysins on *Giardia duodenalis* and specific targeting with anti-*Giardia* antibodies. *Int. J. Parasitol.* **29**, 489-498.
11. Michaels, D. W. (1979). Membrane damage by a toxin from the sea anemone *Stoichactis helianthus*. I. Formation of transmembrane channels in lipid bilayers. *Biochim. Biophys. Acta,* **555**, 67-78.
12. Varanda, W. & Finkelstein, A. (1980). Ion and nonelectrolyte permeability properties of channels formed in planar lipid bilayer membranes by the cytolytic toxin from the sea anemone, *Stoichactis helianthus*. *J. Membr. Biol.* **55**, 203-211.
13. Belmonte, G., Pederzolli, C., Maček, P. & Menestrina, G. (1993). Pore formation by the sea anemone cytolysin equinatoxin II in red blood cells and model lipid membranes. *J. Memb. Biol.* **131**, 11-22.
14. Tejuca, M., Dalla, Serra M., Ferreras, M., Lanio, M. E. & Menestrina, G. (1996). Mechanism of membrane permeabilization by sticholysin I, a cytolysin isolated from venom of the sea anemone *Stichodactyla helianthus*. *Biochemistry,* **35**, 14947-14957.
15. de los Rios, V., Mancheño, J. M., Lanio, M. E., Oñaderra, M. & Gavilanes, J. G. (1998). Mechanism of the leakage induced on lipid model membranes by the hemolytic protein sticholysin II from the sea anemone *Stichodactyla helianthus*. *Eur. J. Biochem.* **252**, 284-289.
16. de los Rios, V., Mancheño, J. M., Martinez del Pozo, A., Alfonso, C., Rivas, G., Oñaderra, M. & Gavilanes, J. G. (1999). Sticholysin II, a cytolysin from the sea anemone *Stichodactyla helianthus*, is a monomer-tetramer associating protein. *FEBS Letters,* **455**, 27-30.
17. Martin-Benito, J., Gavilanes, F., de los Rios, V., Mancheño, J. M., Fernández, J. J. & Gavilanes, J. G. (2000). Two-dimensional crystallization on lipid monolayers and three-dimensional structure of sticholysin II, a cytolysin from the sea anemone *Stichodactyla helianthus*. *Biophys. J.* **78**, 3186-3194.
18. Anderluh, G., Barlič, A., Potrich, C., Maček, P. & Menestrina, G. (2000). Lysine 77 is a key residue in aggregation of equinatoxin II, a pore-forming toxin from sea anemone *Actinia equina*. *J. Membr. Biol.* **173**, 47-55.
19. Bernheimer, A. W. & Avigad, L. S. (1976). Properties of a toxin from the sea anemone *Stoichactis helianthus*, including specific binding to sphingomyelin. *Proc. Natl Acad. Sci. USA,* **73**, 467-471.
20. Linder, R., Bernheimer, A. W. & Kim, K. S. (1977). Interaction between sphingomyelin and a cytolysin from the sea anemone *Stoichactis helianthus*. *Biochim. Biophys. Acta,* **467**, 290-300.
21. Caaveiro, J. M. M., Echabe, I., Gutiérrez-Aguirre, I., Nieva, J. L., Arrondo, J. L. & González-Mañas, J. M. (2001). Differential interaction of equinatoxin II with model membranes in response to lipid composition. *Biophys. J.* **80**, 1343-1353.
22. Maček, P., Zecchini, M., Pederzolli, C., Dalla, Serra M. & Menestrina, G. (1995). Intrinsic tryptophan fluorescence of equinatoxin II, a pore-forming polypeptide from the sea anemone *Actinia equina* L, monitors its interaction with lipid membranes. *Eur. J. Biochem.* **234**, 329-335.
23. Maček, P. & Lebez, D. (1988). Isolation and characterization of three lethal and hemolytic toxins from the sea anemone *Actinia equina* L. *Toxicon,* **26**, 441-451.
24. Norton, R. S., Bobek, G., Ivanov, J. O., Thomson, M., Fiala-Beer, E., Moritz, R. L. & Simpson, R. J. (1990). Purification and characterisation of proteins with cardiac stimulatory and haemolytic activity from the anemone *Actinia tenebrosa*. *Toxicon,* **28**, 29-41.
25. Simpson, R. J., Reid, G. E., Moritz, R. L., Morton, C. & Norton, R. S. (1990). Complete amino acid sequence of tenebrosin-C, a cardiac stimulatory and haemolytic protein from the sea anemone *Actinia tenebrosa*. *Eur. J. Biochem.* **190**, 319-328.

26. Belmonte, G., Menestrina, G., Pederzolli, C., Krizaj, I., Gubenšek, F., Turk, T. & Maček, P. (1994). Primary and secondary structure of a pore-forming toxin from the sea anemone *Actinia equina* L., and its association with lipid vesicles. *Biochim. Biophys. Acta,* **1192**, 197-204.
27. Anderluh, G., Križaj, I., Štrukelj, B., Gubenšek, F., Maček, P. & Pungerčar, J. (1999). Equinatoxins, pore-forming proteins from the sea anemone *Actinia equina*, belong to a multigene family. *Toxicon,* **37**, 1391-1401.
28. Wang, Y., Chua, K. L. & Khoo, H. E. (2000). A new cytolysin from the sea anemone, *Heteractis magnifica*: isolation, cDNA cloning and functional expression. *Biochim. Biophys. Acta,* **1478**, 9-18.
29. Lanio, M. E., Morera, V., Alvarez, C., Tejuca, M., Gomez, T. F. *et al* (2001). Purification and characterization of two hemolysins from *Stichodactyla helianthus*. *Toxicon,* **39**, 187-194.
30. Poklar, N., Lah, J., Salobir, M., Maček, P. & Vesnaver, G. (1997). pH and temperature-induced molten globule-like denatured states of equinatoxin II: a study by UV-melting, DSC, far- and near-UV CD spectroscopy, and ANS fluorescence. *Biochemistry,* **36**, 14345-14352.
31. Poklar, N., Fritz, J., Maček, P., Vesnaver, G. & Chalikian, T. V. (1999). Interaction of the pore-forming protein equinatoxin II with model lipid membranes: a calorimetric and spectroscopic study. *Biochemistry,* **38**, 14999-15008.
32. Malovrh, P., Barlič, A., Podlesek, Z., Maček, P., Menestrina, G. & Anderluh, G. (2000). Structure-function studies of tryptophan mutants of equinatoxin II, a sea anemone pore-forming protein. *Biochem. J.* **346**, 223-232.
33. Menestrina, G., Cabiaux, V. & Tejuca, M. (1999). Secondary structure of sea anemone cytolysins in soluble and membrane bound form by infrared spectroscopy. *Biochem. Biophys. Res. Commun.* **254**, 174-180.
34. Anderluh, G., Barlič, A., Podlesek, Z., Maček, P., Pungerčar, J. & Gubenšek, F. *et al*. (1999). Cysteine-scanning mutagenesis of an eukaryotic pore-forming toxin from sea anemone. Topology in lipid membranes. *Eur. J. Biochem.* **263**, 128-136.
35. Zhang, W., Hinds, M. G., Anderluh, G., Hansen, P. E. & Norton, R. S. (2000). Sequence-specific resonance assignments of the potent cytolysin equinatoxin II. *J. Biomol. NMR,* **18**, 281-282.
36. Brünger, A. T., Adams, P. D., Clore, G. M., DeLano, W. L., Gros, P. & Grosse-Kunstleve, R. W. *et al*. (1998). Crystallography & NMR system: A new software suite for macromolecular structure determination. *Acta Crystallog. sect. D, Biol. Crystallog.* **54**, 905-921.
37. Güntert, P., Mumenthaler, C. & Wüthrich, K. (1997). Torsion angle dynamics for NMR structure calculation with the new program DYANA. *J. Mol. Biol.* **273**, 283-298.
38. Linge, J. P. & Nilges, M. (1999). Influence of non-bonded parameters on the quality of NMR structures: a new force field for NMR structure calculation. *J. Biomol. NMR,* **13**, 51-59.
39. Laskowski, R. A., Rullman., J. A. C., MacArthur, M. W., Kaptein, R. & Thornton, J. M. (1996). AQUA and PROCHECK-NMR: programs for checking the quality of protein structures solved by NMR. *J. Biomol. NMR,* **8**, 477-486.
40. Athanasiadis, A., Anderluh, G., Maček, P. & Turk, D. (2001). Crystal structure of the soluble form of equinatoxin II, a pore-forming toxin from the sea anemone *Actinia equina*. *Structure,* **9**, 341-346.
41. Lu, G. G. (2000). TOP: a new method for protein structure comparisons and similarity searches. *J. App. Crystallog.* **33**, 176-183.
42. Yao, S., Smith, D. K., Hinds, M. G., Zhang, J-G., Nicola, N. A. & Norton, R. S. (2000). Backbone dynamics measurements on leukemia inhibitory factor, a rigid four-helical bundle cytokine. *Protein Sci.* **9**, 671-682.
43. Holm, L. & Sander, C. (1999). Protein folds and families: sequence and structure alignments. *Nucl. Acids Res.* **27**, 244-247.
44. Gibrat, J. F., Madej, T., Spouge, J. L. & Bryant, S. H. (1997). The VAST protein structure comparison method. *Biophys. J.* **72**, MP298.
45. Stintzi, A., Heitz, T., Prasad, V., Wiedemann-Merdinoglu, S., Kauffmann, S., Geoffroy, P. *et al*. (1993). Plant ''pathogenesis-related'' proteins and their role in defense against pathogens. *Biochimie,* **75**, 687-706.
46. Rey, F. A., Heinz, F. X., Mandl, C., Kunz, C. & Harrison, S. C. (1995). The envelope glycoprotein from tick-borne encephalitis virus at 2 Å resolution. *Nature,* **375**, 291-298.
47. Anderluh, G., Pungerčar, J., Križaj, I., Štrukelj, B., Gubenšek, F. & Maček, P. (1997). N-terminal truncation mutagenesis of equinatoxin II, a pore-forming protein from the sea anemone *Actinia equina*. *Protein Eng.* **10**, 751-755.
48. Killian, J. A. & von Heijne, G. (2000). How proteins adapt to a membrane-water interface. *Trends Biochem. Sci.* **25**, 429-434.
49. Yang, L., Harroun, T. A., Weiss, T. M., Ding, L. & Huang, H. W. (2001). Barrel-stave model or toroidal model? A case study on melittin pores. *Biophys. J.* **81**, 1475-1485.
50. Valcarcel, C. A., Dalla, Serra M., Potrich, C., Bernhart, I., Tejuca, M., Martinez, D. *et al*. (2001). Effects of lipid composition on membrane permeabilization by sticholysin I and II, two cytolysins of the sea anemone *Stichodactyla helianthus*. *Biophys. J.* **80**, 2761-2774.
51. Song, L., Hobaugh, M. R., Shustak, C., Cheley, S., Bayley, H. & Gouaux, J. E. (1996). Structure of staphylococcal α-hemolysin, a heptameric transmembrane pore. *Science,* **274**, 1859-1866.
52. Poklar, N., Völker, J., Anderluh, G., Maček, P. & Chalikian, T. V. (2001). Acid- and base-induced conformational transitions of equinatoxin II. *Biophys. Chem.* **90**, 103-121.
53. van der Goot, F. G., Gonzalez-Manas, J. M., Lakey, J. H. & Pattus, F. (1991). A ''molten-globule'' membrane-insertion intermediate of the pore-forming domain of colicin A. *Nature,* **354**, 408-410.
54. Simons, K. & Ikonen, E. (2000). How cells handle cholesterol. *Science,* **290**, 1721-1726.
55. Anderluh, G., Pungerčar, J., Štrukelj, B., Maček, P. & Gubenšek, F. (1996). Cloning, sequencing, and expression of equinatoxin II. *Biochem. Biophys. Res. Commun.* **220**, 437-442.
56. Sattler, M., Schleucher, J. & Griesinger, C. (1999). Heteronuclear multidimensional NMR experiments for the structure determination of proteins in solution employing pulsed field gradients. *Prog. NMR Specy,* **34**, 93-158.

57. Bartels, C., Xia, T., Billeter, M., Güntert, P. & Wüthrich, K. (1995). The program XEASY for computer-supported NMR spectral-analysis of biological macromolecules. *J. Biomol. NMR,* **6**, 1-10.
58. Skelton, N. J., Palmer, A. G., Akke, M., Kordel, J., Rance, M. & Chazin, W. J. (1993). Practical aspects of 2-dimensional proton-detected N-15 spin relaxation measurements. *J. Magn. Reson. ser. B,* **102**, 253-264.
59. Vuister, G. W. & Bax, A. (1993). Quantitative J correlation - a new approach for measuring homonuclear 3-bond J(HNHα) coupling-constants in N-15-enriched proteins. *J. Am. Chem. Soc.* **115**, 7772-7777.
60. Luginbühl, P., Szyperski, T. & Wüthrich, K. (1995). Statistical basis for the use of $^{13}C\alpha$ chemical shifts in protein structure determination. *J. Magn. Reson. ser. B,* **109**, 229-233.
61. Ludvigsen, S. & Poulsen, F. M. (1992). Positive ϕ-angles in proteins by nuclear magnetic resonance and distance geometry. *J. Biomol. NMR,* **2**, 227-233.
62. Koradi, R., Billeter, M. & Wüthrich, K. (1996). MOLMOL: a program for display and analysis of macromolecular structures. *J. Mol. Graph.* **14**, 51-55.
63. Nicholls, A., Sharp, K. A. & Honig, B. (1991). Protein folding and association: insights from the interfacial and thermodynamic properties of hydrocarbons. *Proteins: Struct. Funct. Genet.* **11**, 281-296.

Edited by M. F. Summers

(Received 14 September 2001; received in revised form 24 November 2001; accepted 24 November 2001)